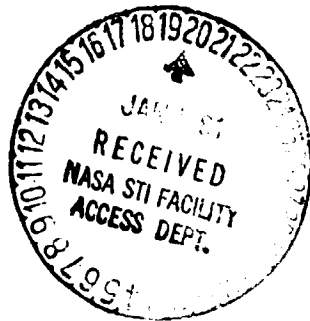# N O T I C E

THIS DOCUMENT HAS BEEN REPRODUCED FROM MICROFICHE. ALTHOUGH IT IS RECOGNIZED THAT CERTAIN PORTIONS ARE ILLEGIBLE, IT IS BEING RELEASED IN THE INTEREST OF MAKING AVAILABLE AS MUCH INFORMATION AS POSSIBLE

MUON SPIN ROTATION RESEARCH PROGRAM

VIRGINIA STATE UNIVERSITY
PETERSBURG, VA 23803

SUPPORTED BY NASA GRANT NSG 1342

ANNUAL REPORT - 1980

Carey E. Stronach
Project Director

During 1980 the μSR Research Program at Virginia State University concentrated upon studies of ferromagnetic materials, primarily dilute alloys of iron, and iron crystals under stress. These experiments were done at the TRIUMF cyclotron in Vancouver, British Columbia, and at the SIN cyclotron in Villigen, Switzerland.

We have continued to analyze the data taken at TRIUMF on the temperature dependence of the interstitial magnetic field B_μ observed by the μ^+ in Fe(Mo), Fe(Nb), and Fe(Ti), and the room-temperature studies of Fe(V), Fe(Cr), Fe(Mn), Fe(Ta), and Fe(W).

The Fe(Mo) data indicate that the effect upon the contact hyperfine field in Fe due to the introduction of Mo is considerably less than that expected from pure dilution, and that the μ^+ are attracted to the Mo impurity sites.

The Fe(Nb) data are difficult to interpret because this is a two-phase alloy, $Fe_x \cdot (Fe_2Nb)_{1-x}$. There is a significant change in B_μ with Nb concentration, however, and the impurities are clearly attractive to the μ^+. These results suggest that strain fields may play a role in B_μ, or that there may be weak trapping along grain boundaries.

The Fe(Ti) data, for which precession could clearly be observed only at 468K and above, showed that the Ti impurities are attractive to μ^+, and that the magnitude of B_{hf} is reduced far beyond the amount expected from pure dilution.

The room temperature data show that B_μ is greater than that observed in pure Fe, when Cr, W, or Mo is introduced into the crystal, but is smaller

2

when Ta, Mn, V, or Nb is introduced. There seems to be a correlation with the size of the impurity atom, which further suggests that strain fields may be playing a role.

We have also studied the change in B_μ in Fe with the introduction of Ge and Si. B_μ increases with increasing concentration of both, behaving much like the Fe(Al) alloy. We also found that the shape of the $B_\mu(T)$ curve for Fe(Ge) changes markedly with annealing. The magnitude of B_μ is larger at low temperatures and smaller at high temperatures after the sample has been annealed. This again suggests that strains and defects are playing a role.

All of the experiments described above were done at TRIUMF in collaboration with A. S. Arrott et al. of Simon Fraser University, W. F. Lankford of George Mason University, A. T. Fiory of Bell Laboratories, and W. J. Kossler of the College of William and Mary. A paper on Fe alloyed with the transition elements is in progress and will be included in the next report.

The study of strained Fe crystals showed that when strained to the elastic limit B_μ is reduced by 33 gauss, and the relaxation rate of the precession signal increases by 47%. A more detailed experiment with oriented crystals and a strain apparatus for which the temperature can be varied is being planned for March 1981 at SIN. The preliminary experiment was performed at SIN in collaboration with W. J. Kossler of the College of William and Mary, and B. D. Patterson, P. F. Meier, and W. Kündig of the University of Zürich.

B_μ was measured at room temperature in a number of Fe alloys at SIN. These include Fe(Si), Fe(Ti), Fe(Ge), Fe(Cr), and Fe(Mo). These results are

consistent with those obtained at TRIUMF, and will be incorporated into a future paper. Plots of the precession spectra are included as an appendix to this report.

A paper on "*Current techniques in muon spin rotation experiments*" was accepted by the journal *Nuclear Instruments and Methods* in November 1980. A preprint is included as an appendix to this report.

The principal investigator went to TRIUMF to perform experiments in November 1979, March 1980, August 1980, and November 1980. He also attended the Second International Topical Meeting on Muon Spin Rotation during the August trip. He went to SIN in July 1980 for the strained-Fe crystal and alloy experiments.

One major piece of equipment, an Ortec 934 four-fold constant fraction discriminator, was purchased during the year.

The construction of a low-energy π/μ channel at the Alternate Gradient Synchrotron of Brookhaven National Laboratory is expected to be completed in September 1982. This project was delayed for a year because of problems associated with the ISABELLE facility, but no additional delays are expected. When this beam comes on line we will concentrate our μSR work at Brookhaven and reduce our travel to TRIUMF and SIN. In the meantime, the collaborations at TRIUMF and SIN have been most successful and we expect them to continue in like manner for the next eighteen months.

A part-time graduate student at VSU, Kevin R. Squire, has been working on this project, beginning in November 1980. He is concentrating on data analysis.

The support provided to VSU by NASA through this program, and the interest and concern of the technical monitor, Dr. Jag J. Singh of the Langley Research Center, are warmly appreciated.
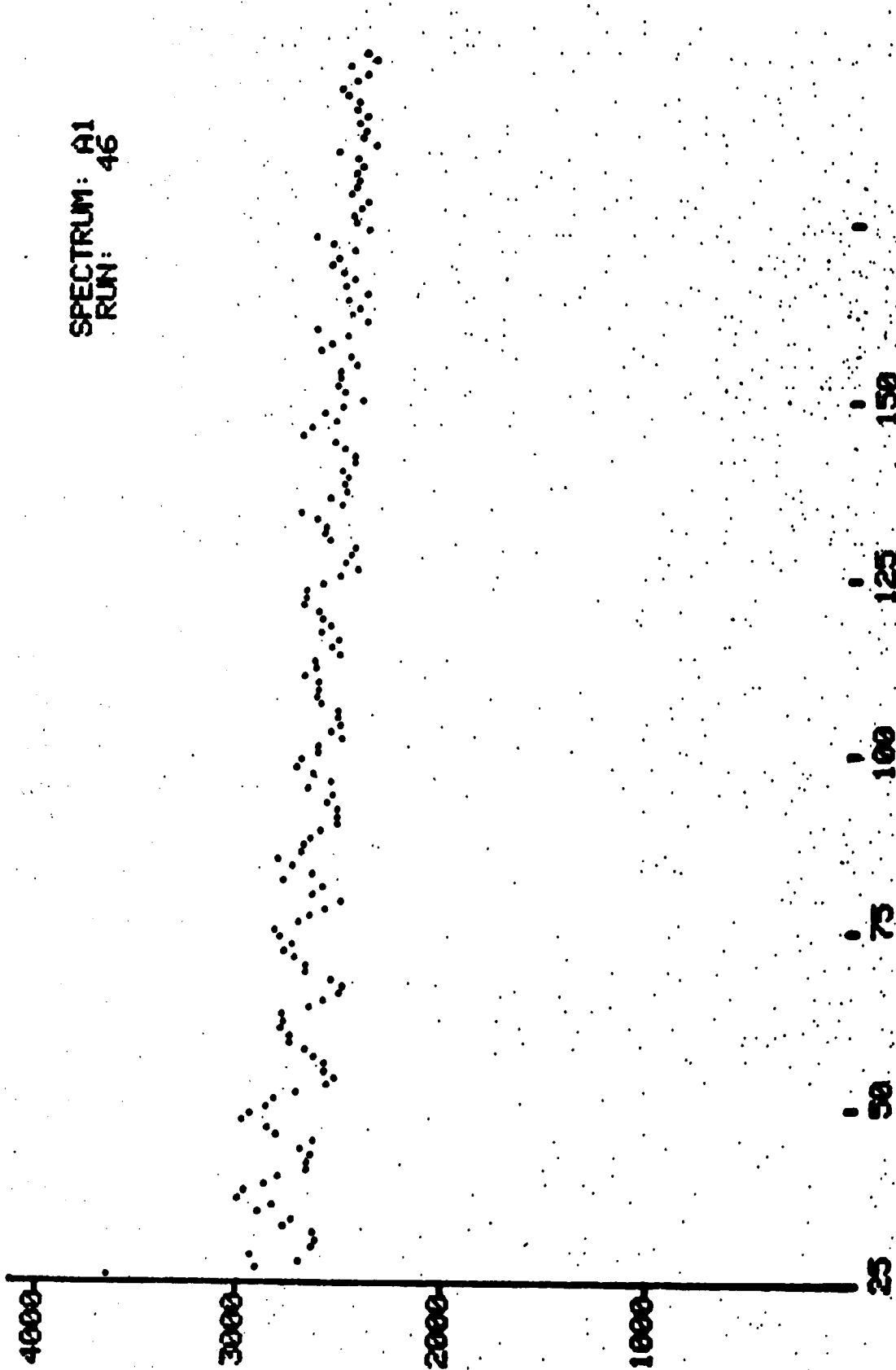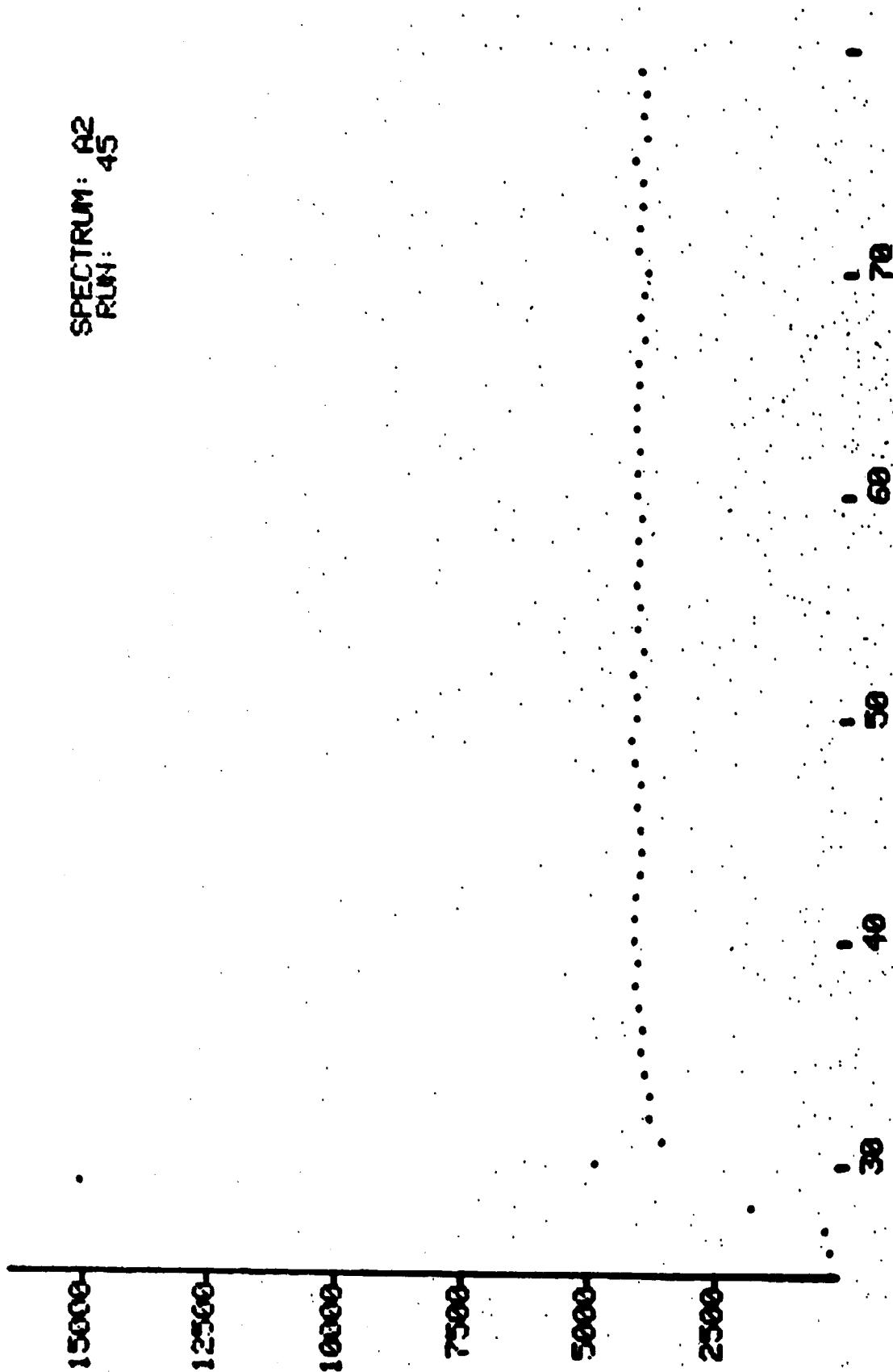
Carey E. Stronach

Project Director
January 15, 1981

5

ATF F2 4%Gz RT

SPECTRUM: A1
RUN: 46

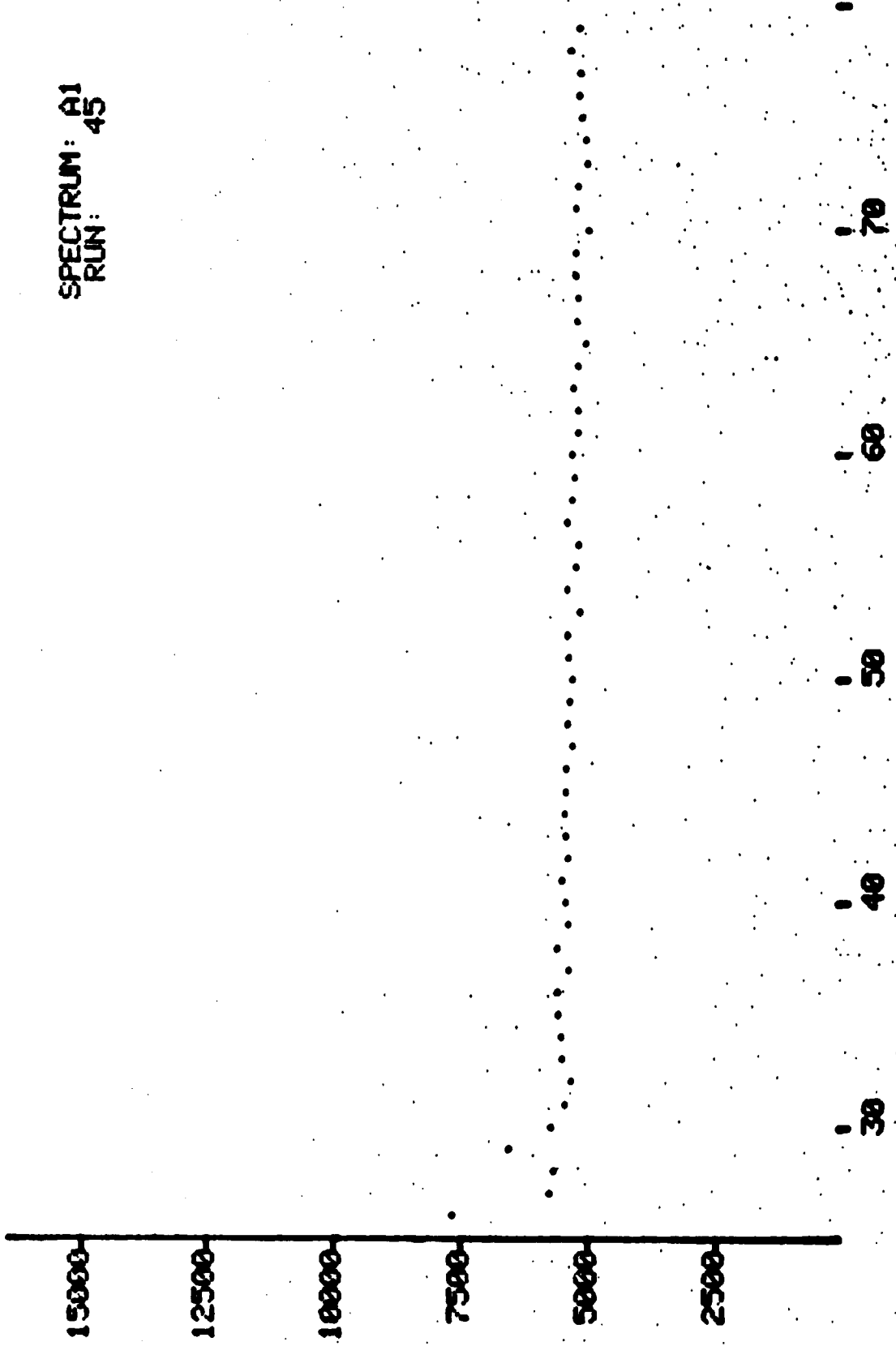$F_2 \ (2\% \ T_i)$ Arnott
RT

SPECTRUM: A2
RUN: 45

$F_2 (2^2 T_i)$ $\dfrac{Arnott}{RT}$

SPECTRUM: A1
RUN: 45

15000

12500

10000

7500

5000

2500

30

40

50

60

70

Arnott Fe 2% Cr
RT

SPECTRUM: A1
RUN: 47

Arrott Fe 2% Cr RT

SPECTRUM: A2
RUN: 47

2000 1500 1000 500

50 100 150 200 250 300

SPECTRUM: A2
RUN: 42

2000

1500

1000

500

0   50   100   150
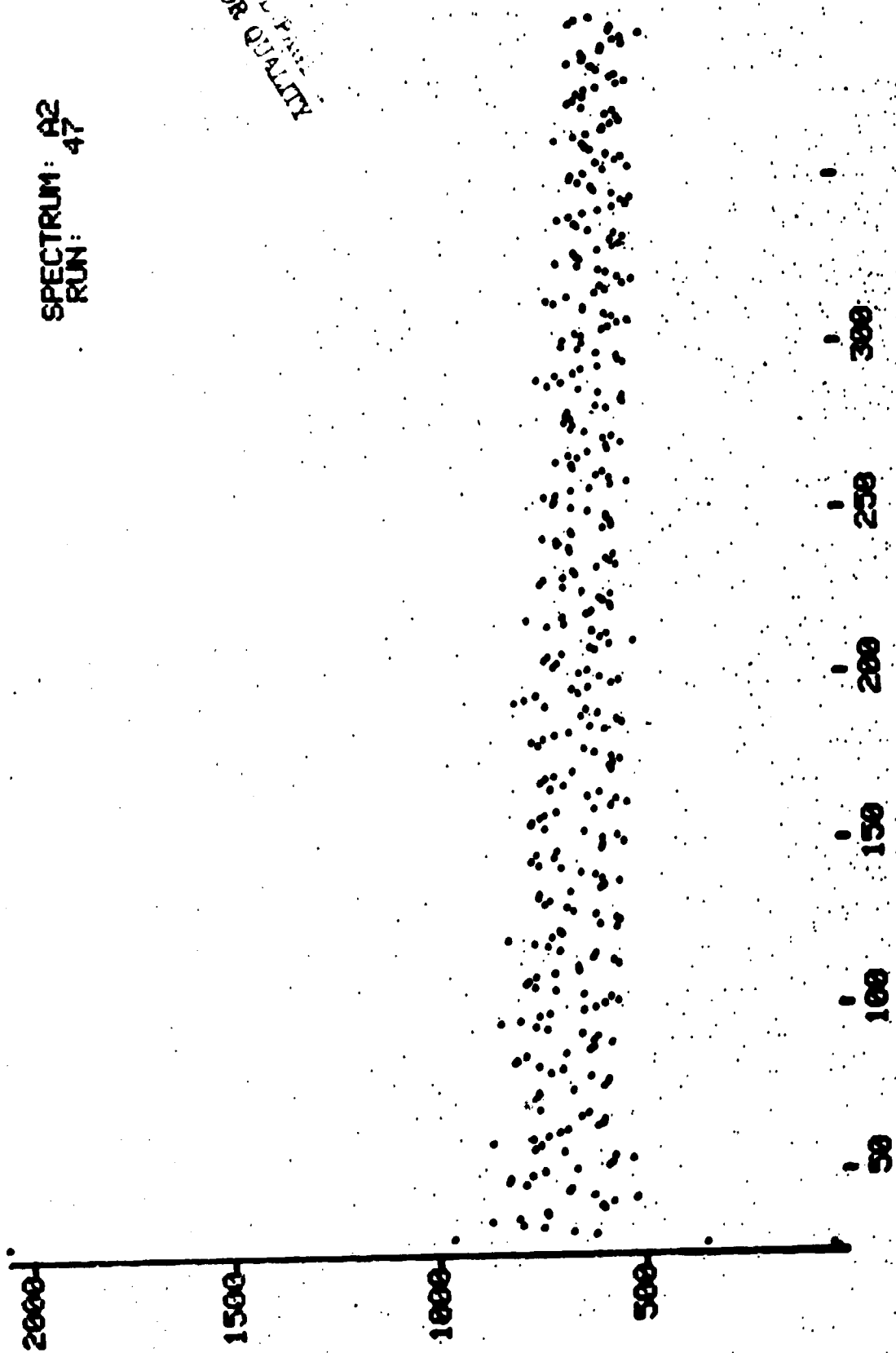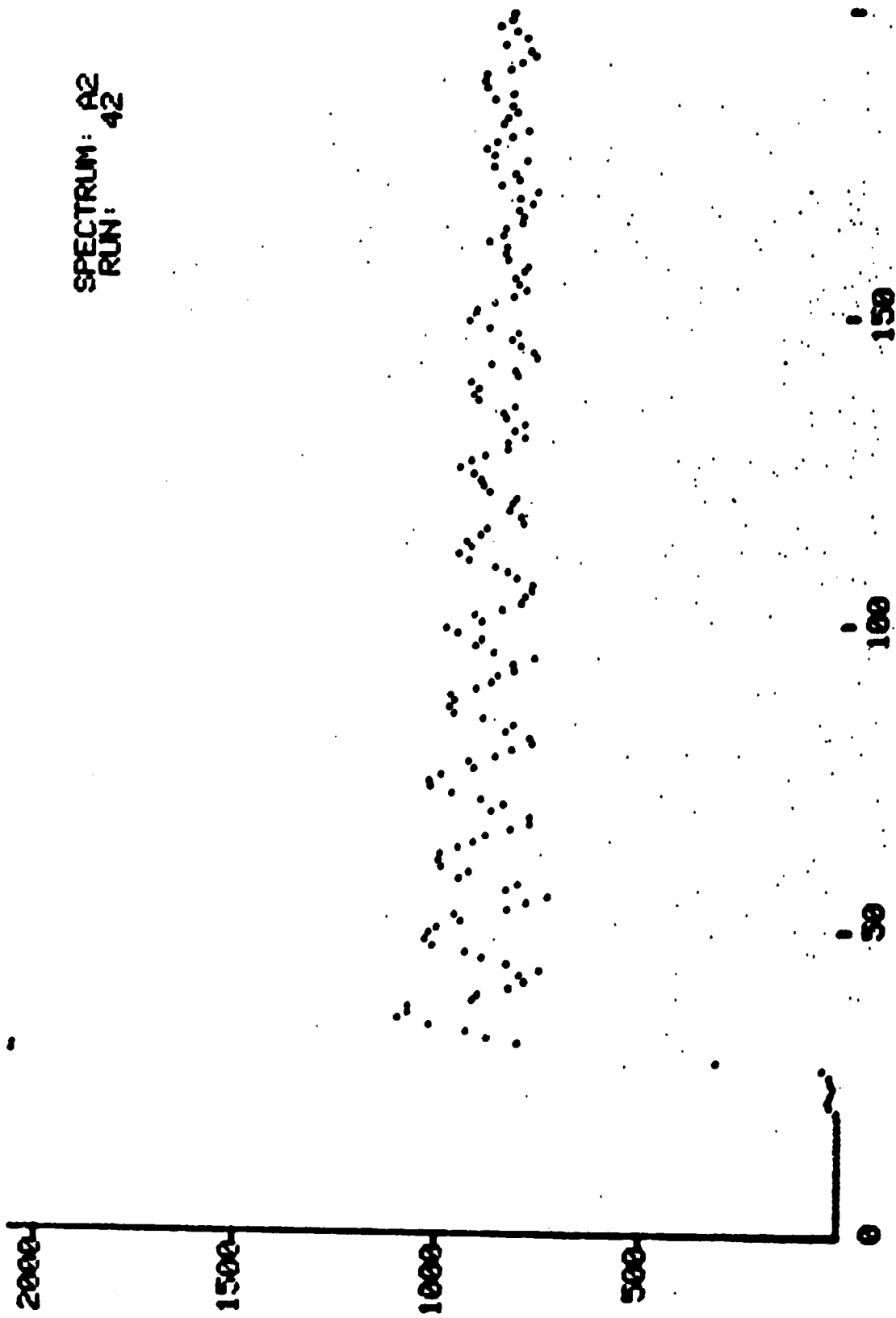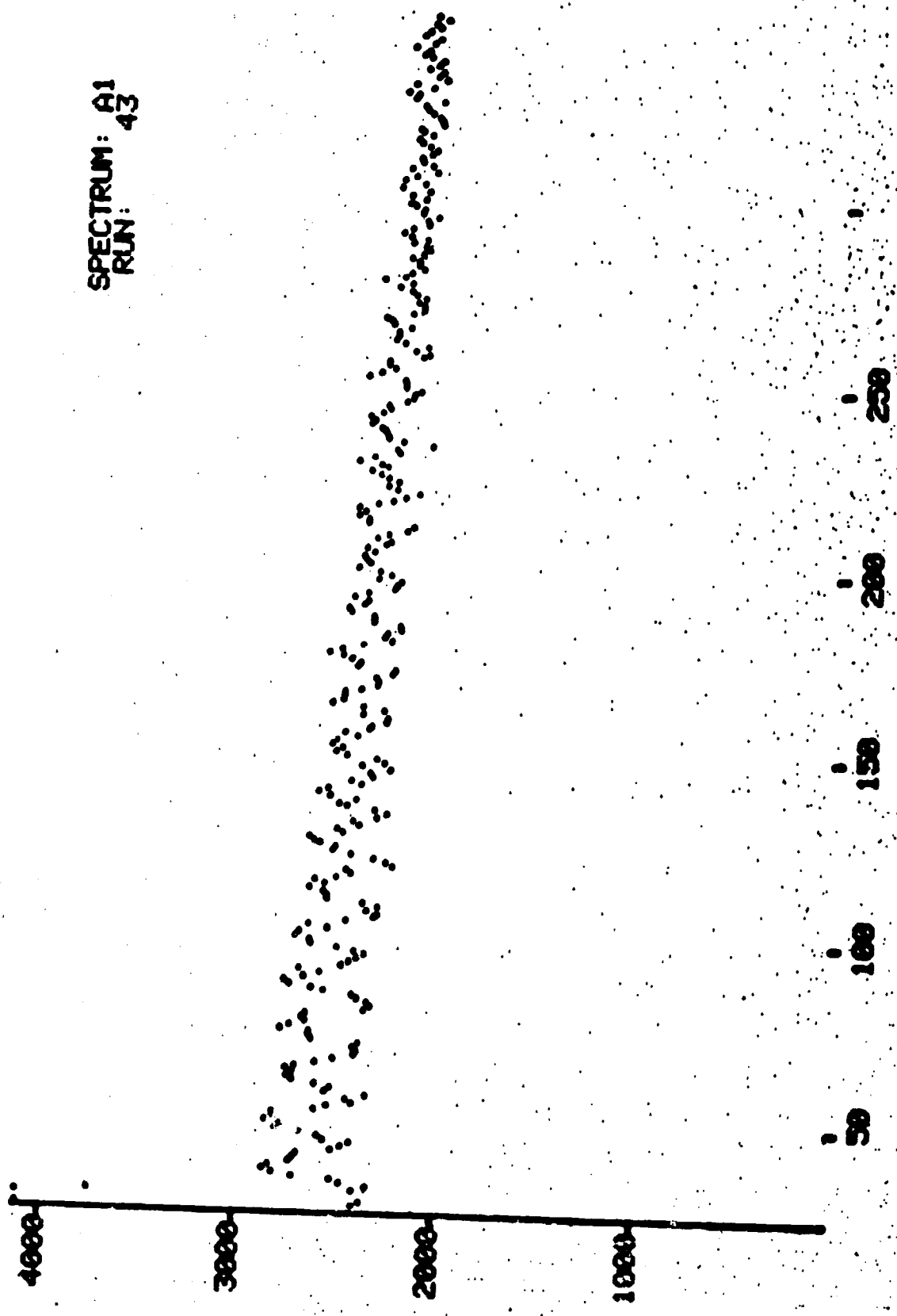
SPECTRUM: A1
RUN: 43

RT

SPECTRUM: A2
RUN: 43

40000

30000

2000

1000

50   100   150   200   250

Fe single crystals
RT

SPECTRUM: A1
RUN: 44

50   100   150   200   250

1000 2000 3000 4000 5000 6000 7000 8000

Fe single crystals
121

SPECTRUM: A2
RUN: 44

ORIGINAL PAGE IS
OF POOR QUALITY
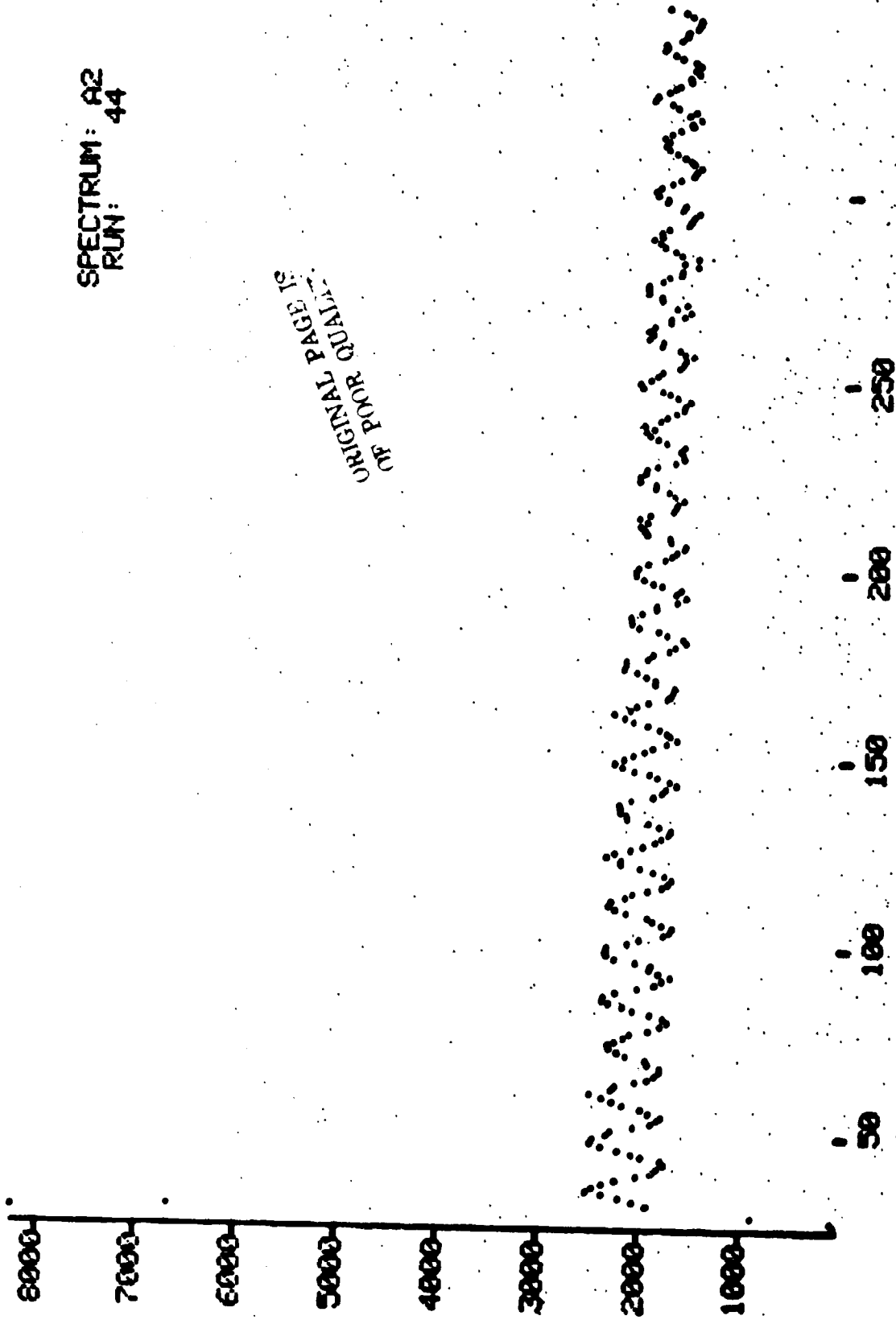
III Fe single crystals RT
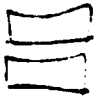
SPECTRUM: A2
RUN: 44
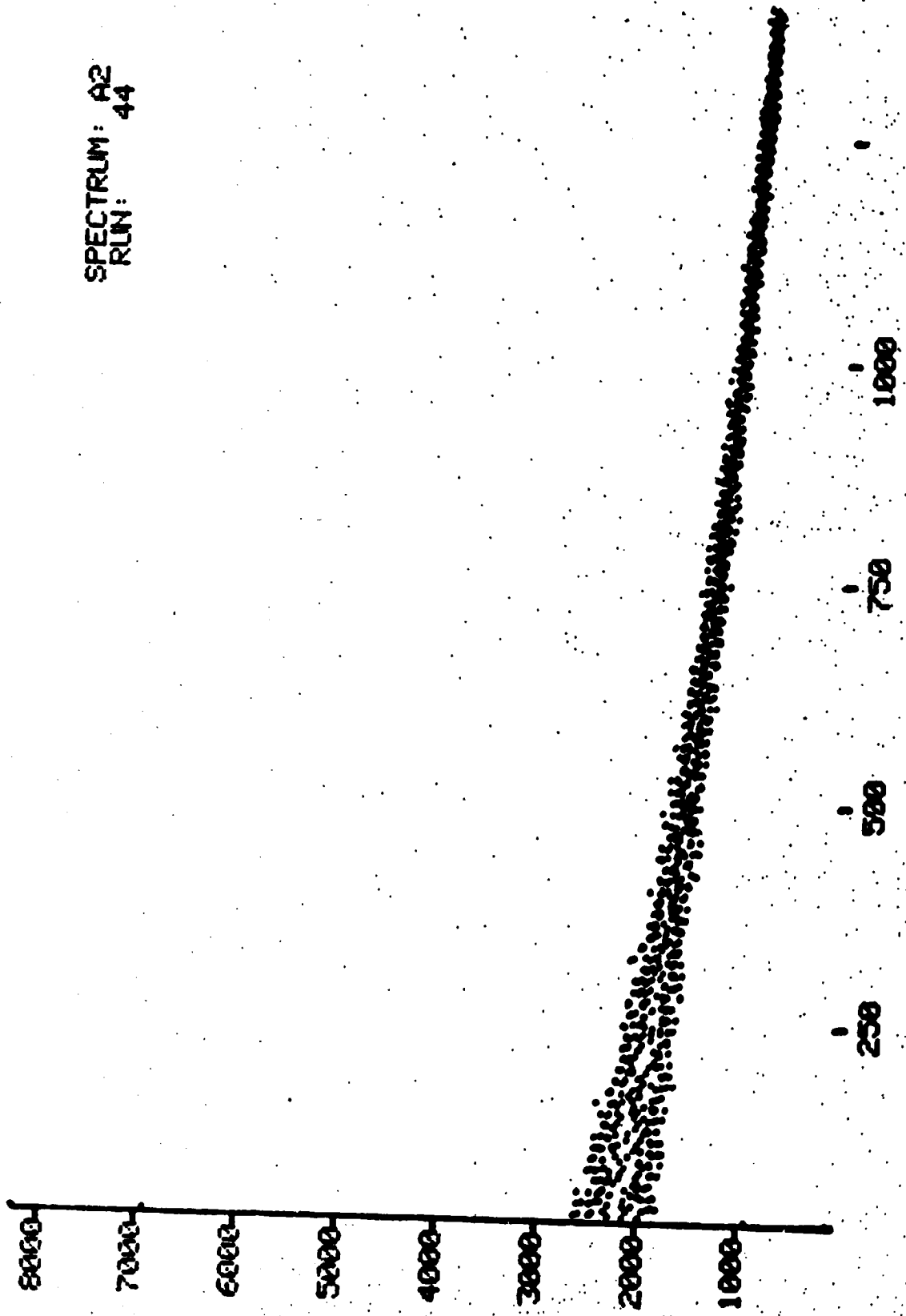
ATF Fe 4% Ge
RT

SPECTRUM: A2
RUN: 46
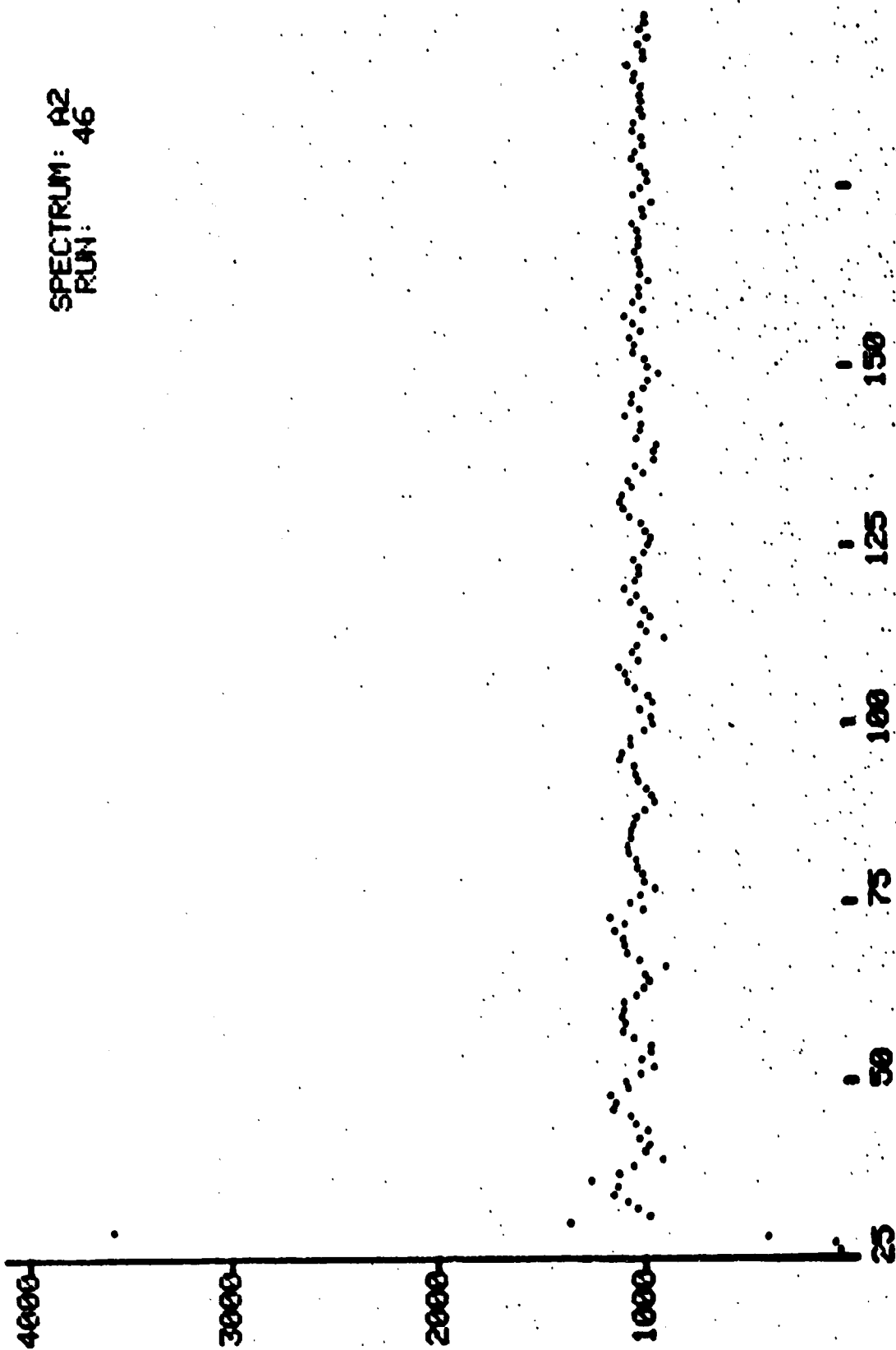
CURRENT TECHNIQUES IN MUON SPIN ROTATION EXPERIMENTS

William F. Lankford
George Mason University, Fairfax, Virginia 22030

Kelvin G. Lynn
Brookhaven National Laboratory, Upton, New York 11973

William J. Kossler
The College of William and Mary, Williamsburg, Virginia 23186

Anthony T. Fiory and R. Paul Minnich
Bell Laboratories, Murray Hill, New Jersey 07974

Cary E. Stronach
Virginia State University, Petersburg, Virginia 23803

A B S T R A C T

Experimental techniques in muon spin rotation are described and the principles governing the measurement and optimization of the precession signals are analyzed. Emphasis is placed on the description of the important experimental considerations for performing such experiments and the accessibility of this technique to condensed matter and muonium chemistry research.

Current Techniques in Muon Spin Rotation Experiments

1. Introduction

In recent years there has been rapid growth in muon spin rotation (µSR) research with an accompanying increase in the sophistication of the experimental techniques being applied. Excellent reviews of basic µSR theory and application to current problems are available.[1,2] However, as this approach to the study of solids and liquids becomes increasingly widespread, a systematic review of current experimental techniques and limitations should be useful to experimenters considering the use of µSR in the characterization of materials under study by other means. It is also hoped that this review will prove useful to those who are considering entering the growing field of µSR research.

Briefly, µSR is carried out with a beam of spin polarized muons obtained from the decay of pions produced in the production target of a proton accelerator[3] and stopped in the sample under investigation. The precession of the muon spin in the local magnetic field of the sample and its subsequent decay provide a non-destructive probe of the solid state based on principles similar to those of perturbed angular correlations. This application of nuclear physics techniques to the study of solid state and chemical physics provides information that is also analogous to that obtained by nuclear magnetic resonance (NMR) and Mössbauer experiments. We will describe the basic µSR technique in some detail and discuss some of the capabilities of currently available instrumentation as well as ways to optimize the sample-dependent contributions to the amplitude of the precession signal.

Fundamentals

The usefulness of the muon in μSR investigations depends on its parity violating decay:

$$\mu^{\pm} \rightarrow e^{\pm} + \nu + \bar{\nu} \tag{1}$$

with a lifetime of 2.19713×10^{-6} sec.

The angular distribution of the electrons or positrons is given by

$$R(\theta) \propto 1 + a\cos\theta \tag{2}$$

which results from weak interaction theory as described for example in Frauenfelder and Henley's text.[4] The decay asymmetry has a value of $a = 1/3$ when all positron energies are included. This distribution and the shape of the positron energy spectrum are shown in Figures 1a & 1b.[5]

For bare muons the distribution precesses in a local magnetic field with the Larmor frequency:

$$\omega = \frac{2\mu_{\mu}B}{\hbar} \tag{3}$$

where μ_{μ} = the muon magnetic moment.

and

$$\frac{\mu_{\mu}}{\hbar} = 42.568 \frac{kHz}{Gauss} \tag{4}$$

The precession frequency of the muon spin then gives the average local magnetic field, B. However, in materials, different muon processes are encountered depending on the electron density and magnetic character of the host. In non-magnetic conductors the electron spin correlation time is sufficiently short that the muon behaves as though it were nearly bare, and the precession frequency is given by the above expression.[6]

On the other hand, in insulators or semiconductors muonium ($\mu^{+} e^{-}$) is formed, which precesses at a rate:

$$\omega = \frac{\mu_m B}{\hbar} \qquad\qquad (5)$$

where μ_m is the muonium magnetic moment

and $\qquad \dfrac{\mu_m}{\hbar} = 1.394 \dfrac{MHz}{Gauss} \qquad\qquad (6)$

Here the muonium magnetic moment is governed primarily by the larger magnetic moment of the electron. The muonium frequency is easily detected with modern instrumentation; for example, Gurevich, et al[7] have reported muonium precession in ice, quartz, and other materials.

A survey of μSR applications to the study of chemical bonding, reaction rates and other areas of muon chemistry is available in a recent review paper,[8] which includes the use of gaseous and liquid targets.

3. The Beams

The muon beams used to date for μSR originate as secondary beams from the production targets of intermediate energy (500-800 Mev) proton accelerators. Major facilities where these beams are available are listed in Table 1. Included also are the estimated fluxes from a proposed beam at the Brookhaven Alternate Gradient Synchrotron.[9] The general beam layout is shown in Figure 2.

At each of these facilities it is possible to produce muon beams of two distinct types. The first, which has been used for the vast majority of μSR experiments, is the in-flight pion decay beam. To produce this beam, protons from a cyclotron or linac strike a target producing a flux of pions and other secondaries. These pions are magnetically collected by quadrupole magnets into a long solenoid or long channel of additional quadrupoles. The pions, with their relatively short lifetime of 2.6×10^{-8} sec, decay into muons according to the expression:

3

$$\pi^{\pm} \rightarrow \mu^{\pm} + \upsilon \ (\bar{\upsilon}).$$

Those muons which are emitted and collected in the forward cone, relative to the pion's velocity, comprise a high momentum component, while those emitted in the backward direction, a lower momentum component. At the end of the channel bending magnets provide the needed beam separation and momentum selection to focus the desired muon beam onto the target. Typically, the forward beam is the more intense while the backward beam is more easily separated from the positive pions and thus provides less background contamination in the data. Muons in these beams range from 50 MeV/c to 150 MeV/c and are slowed by degraders to stop in the sample under study. Polyethylene (CH_4) is commonly used as degrader material, however, variable thickness water degraders conveniently allow rapid range curves and fine adjustments. Beam transport efficiency has been improved with the use of a helium filled bag along the path. However, transport through the experimental apparatus may be in air.

The second type of beam is the surface or Arizona beam named from the design of the first such beam used on the Berkeley 184 inch synchrocyclotron.[10,11] The production geometry is shown in Figure 3. The incident protons traverse the long dimensions of the target producing pions along its path, many of which come to rest in the target. Those pions very near the targets' side surface decay into muons which have enough energy to leave the target to be collected into a beam. Several bends are needed in the magnetic transport system to reduce the high flux of positrons and electrons; however, essentially 100% polarized muon beams are obtained with approximately 30 MeV/c momentum. High fluxes and small penetration distances into the sample result in high stopping densities, allowing very small samples to be

used. The lower muon energy requires beam transport in vacuum with a thin window at the channel end.

4. Transverse Field Measurements

The µSR experiments with positive muons may be divided into two categories depending on whether the applied magnetic field is parallel or transverse to the predominant spin polarization of the incident beam. In the latter case the semiclassical Larmor precession model describes the dynamics of the process. A basic detector arrangement for the transverse field measurements is shown in Figure 4. The B2 M F coincidence, specifying a muon stopped in the target, provides the start signal for a high-frequency clock or a time-to-amplitude converter (TAC). The stop signal for the clock or TAC is provided by a subsequent positron detected in the forward detector F, or the annular detector A. B1 is used for pile-up rejection as discussed in the next section. The monitor detector, M, which specifies muons entering the target, must mask the target dimensions and be smaller than the blank in the center of the annular detector, A. The use of an annular detector for the backward positron permits a minimum dead time of approximately 10 ns between the stopped muon and the first positrons detected. In the forward detector, F, the dead time is limited by the width of the pulse used to veto a muon passing through the target, and is approximately 10-20 ns wide.

The logic diagram shown in Figure 5 illustrates the basic data collection system. When moderately intense muon beams are available, logic requirements must be set to ensure that the muon in the target which triggered the start of the TAC is unambiguously associated with the stop signal from its decay positron. They may be done most simply by using a pile-up gate for B1 and M

and also for F and A. If one muon is detected within a preset time of another
(approximately four muon lifetimes in our case), the gate on B1 or M provides
a pulse to inhibit the TAC. The gate on F or A further reduces the ambiguity
by inhibiting the TACs if two positrons are detected within a time span of
four muon lifetimes.

With this system the dead time between the stopped muon and the positron
in the upstream positron detector, B, is limited by time jitter and walk in
the signals and by discriminator dead time. The walk may be reduced with the
use of constant friction timing discriminators to obtain minimum dead time
when it is desired to measure rapid depolarization rates. With these units a
minimum dead time of 5.0 ns between successive pulses has been achieved. As
there are very few back scattered muons a veto is not required for detector
A. Even though the forward detector, F, is dead time limited, it has the
advantage of larger count rate because of its potentially greater solid angle.

In order to establish a true time zero for the stopped muon, which allows
extrapolation to determine a true initial phase or asymmetry of the
oscillations, the coincidence vetos, F, and, B1 or M, can be removed. This
permits the straight through muons to be detected providing a prompt spike in
the spectrum. Time calibration and linearity checks can be accomplished with
a standard TAC calibrator or by using a time mark generator in random
coincidence with a beam particle pulse as the start and stop signals for the
TAC. Overall resolution of the system on the order of 0.5 ns can be achieved
with the use of small area detectors.[2]

In very intense beams which can be pulsed for short durations,
stroboscopic techniques (Section 10) permit rapid data rates by allowing more
than one muon in the target at a time. Here resolution depends on the width
of the beam pulse.

6

Typical time histograms for the time-differential method is shown in Figure 6 for a vanadium sample at three different temperatures. The important parameters of the data are determined by least squares fitting to the function

$$N(t) = N(0)e^{-t/\tau_\mu} \left[1 + aP(t) \cos(\omega t + \theta) \right] + Bkg \quad (8)$$

where

τ_μ is the muon lifetime

ω is the radial precession frequency,

θ is the geometry-dependent phase angle,

Bkg   is the random background,

a   is an asymmetry parameter dependent on the experimental setup, and

P(t)   is the time dependent depolarization, sometimes approximated as a Gaussian $P(t) = P_o e^{-o^2 t^2}$
or exponential $P(t) = P_o e^{-\lambda t}$ form.

The initial asymmetry P(0) in the oscillations is defined at $t = 0$ and hereafter referred to simply as the asymmetry. It can be determined by least squares fitting the parameter $A = aP(0)$ in the above equation. This asymmetry is, of course, dependent on several experimental parameters as we discuss later. It is important to increase this parameter as much as possible to minimize the experimental run time needed to obtain accurate values of the precession frequency and the depolarization. For an asymmetry of 16% with 4 million events in a 2048-channel time histogram (8μs), the important experimental parameters have been determined to about 0.1% accuracy in the depolarization rate and 0.1% accuracy in the precession frequency in non-

7

magnetic metals. With a stop rate of 7000 muons sec^{-1} this requires about 40 minutes of running time with an event rate of 2000 sec^{-1} and a conversion efficiency of 75% routing into two halves of the pulse height analyzer. Rapid data analysis with an on-line computer is employed to permit selection of additional data points for interesting temperature or field regions while the sample is still in place. Using the PDP 11/10, a non-linear least squares fit over 1800 channels can be obtained in about 12 minutes.

In both conductors and insulators the measurement of the precession frequency allows determination of the local magnetic field in the sample. In metals carefully designed experiments permit the measurement of Knight shifts.[12] Useful information is also obtained from the depolarization rate, which corresponds to the line width of NMR signals. For example, the muon depolarization can result from the dephasing effects of inhomogeneous nuclear dipolar fields as the muon resides at a particular site. Recent results have suggested that the mechanism of μ^+ diffusion is becoming better understood theoretically.[13,14] In particular, the role of defects is found to be significant. It is apparent that μSR should be a highly sensitive probe in the study of impurity complexes in metals.[15]

5. The Longitudinal Field Technique

In longitudinal field μSR the magnetic field is applied along the muon spin direction. Here the acronym is more accurately read muon spin relaxation and the quantity measured is the depolarization of the spin ensemble, analogous to the longitudinal relaxation rate T_1 of NMR.

A longitudinal relaxation function has been introduced by Yamazaki[16,17] in which ideally the depolarization is given by:

$$G_1(t) = \frac{N_F(0) + N_B(0)}{N_F(0) - N_B(0)} \cdot \frac{N_F(t) - N_B(t)}{N_F(t) + N_B(t)} \qquad (9)$$

where N_F and N_B are intensities of decay positions in the forward and backward directions respectively. This assumes forward and backward counting efficiencies are equal and that the background intensities have been subtracted. A typical detector arrangement to measure these quantities is shown in Figure 7. Here a B2 B1 M μ coincidence denoting a stopped muon, followed by a signal in one of the two annular detectors gives the rates in the above equation.

The measurements of interest are due to the perturbations in muon spin orientation by tranverse field components which induce spin transitions between the forward and backward directions. The effect of a longitudinal field on the depolarization provides useful information on the depolarization mechanism. Local atomic dipolar fields, nuclear moments, diffusion rates and electric field gradients are among the effects that have been studied by this technique.

If the muon is stopped in an insulator and muonium is formed, the μ^+e^- hyperfine field in the sample may be studied. The transitions here are given by the Breit-Rabi formula where the transition energies are magnetic field dependent. Recent work by Brown, et al[18] at LAMPF has successfully studied hyperfine transitions of muonium in quartz induced by an applied intense rf magnetic field.

6. The Detectors and Radiation Background

Most of the detectors presently used in µSR experiments are plastic scintillators coupled with fast photomultiplier tubes. As µSR experiments are

often done in high applied magnetic fields, long light pipes are required between the scintillators and photomultiplier tubes for magnetic isolation. In addition, soft iron and high permeability metal shields are employed over the photomultipliers. To further reduce magnetic interference RCA 8850 photomultiplier tubes are often used. With these tubes it has been found to be advantageous to increase the voltage on the first dynode from the 400 volts supplied by some commercial bases to 600 volts with 100 volts on each of the remaining stages. This reduces transit time dispersion and therefore improves the timing resolution of the system. As higher intensity beams become available, wire chamber detectors will provide improved angular resolution and data collection rates.

Magnetic deflection is another problem for both incoming muons and decay positrons in strong applied transverse magnetic fields. Careful analysis of optimum detector design and placement is needed to optimize count rates over a range of high fields. Heffner et al. at Los Alamos[19] and Uemura at TRIUMF have used fields up to 5 kG. It is an advantage for high intensity beams to use a two-detector telescope for each positron direction to further minimize the background, and is employed at most laboratories today.

The background is attributable primarily to beam scattering, detection inefficiencies, and to random chance coincidence from the background radiation. Normally it can be parameterized by a constant plus a term linear in time. In working with a highly pulsed beam with periodic time structure, the background may reflect the accelerator beam structure. An exponential background decay may also be present from highly pulsed beams, requiring a time dependence of the form

$$Bkg = Ae^{-\gamma t} + B,$$

where Y is the characteristic background constant and A and B are fitted parameters. At low duty factor machines the background may be significantly higher and can produce artifacts in the data which affect the depolarization rate measured in the sample.

In particular when small samples are used, the background from cryostats or heaters may contribute signals which have the same frequency as the sample but different depolarization rates. It may·be necessary to include an additional term in the expression for P(t) in equation 8 to account for this.

An upstream degrader may also be used to absorb the pion contamination in the beam; however, the effect is usually minimal. Of greater importance in reducing background is the placement of the beam collimation and shielding to prevent stray beams from hitting extraneous matter. When a 90° positron detector is used, care must be taken to insure that it does not mask one of the other scintillators. Also, since vacuum ovens or cryostats must be easily inserted and removed during the experiment, considerable care is necessary in counter design.

7. Magnetic Field Homogeneity and Stability

Since much of the value of the μSR technique lies in its sensitivity to inhomogeneities in the local magnetic fields of the sample, it is important to reduce fluctuations and gradients in the applied field as much as possible. While a primary Helmholtz pair may provide the best homogeneity, it is usually necessary to add two additional secondary Helmholtz pairs to nullify stray· magnetic fields from the earth and the transport magnets. An iron core magnet provides good magnetic shielding from stray fields but additional shimming may still be necessary. The shim iron should be of the same susceptability as the

11

core to permit a range of applied fields. Fringe fields from the last focusing quadrupole magnet of the beam line are substantially reduced by attaching a soft iron face plate with an iris for the beam. With all these corrective measures, the field homogeneity for a 23 cm gap "C" magnet can be reduced to ± 10 mG/cm. Over a 6.0 cm target dimension, this contributes only about 1.0 kHz to the depolarization rate in paramagnetic samples.

A Hall probe adjacent to the target has been used to sense drifts or fluctuations in the applied field. A feedback loop, using a bipolar power supply, can be used to provide correction currents to a small coil wound around the magnetic pole tips. With this system field stability of better than one part in 10^4 is readily achieved. Limitations include the temperature stability of the Hall probe.

8. <u>Temperature Control</u>

The problem of maintaining accurate temperature control of the sample over the range from below 2K to above room temperature presents special problems in the beam environment that can be approached in two ways. One is to use a thin window, liquid or gas flow, vacuum cryostat with a wire wound heater near the sample controlled by a feedbck circuit which balances a temperature sensitive calibrated resistor on the sample with an accurate decade resistor. Alternately a closed cycle He refrigerator with the sample mounted on the cold tip has been used. An advantage of the first is that lower temperatures can be obtained (down to 1.7K by pumping), and rapid temperature changes can be achieved. The closed cycle He refrigerator on the other hand has the substantial advantage of economy of operation. At temperatures above 77K, liquid nitrogen offers better cooling rates because of

12

its higher specific heat. Variable temperature control below 2°K can be achieved with a ^{3}He - ^{4}He dilution refrigerator. Hartman, et al have studied Al, Cu, and Al-Mn alloys at temperatures to 30mK with this technique at CERN, maintaining temperature stability with a heater controlled by feedback from a calibrated carbon resistor.[20]

The necessity of thin windows and compact apparatus also places design constraints on the ovens used to maintain samples above room temperature. These systems generally use a resistive heater controlled by a feedback circuit connected to a thermocouple on the sample. There are two basic variations in design. In one, the heater coil, thermocouple and sample are enclosed in a vacuum jacket and sample temperature is maintained by radiation. Considerable care must be exercised to provide uniform radiation to avoid thermal gradients in the sample. The other consists of using a gas flow over the heater coil and then around the sample. Here the gas flow tube and sample chamber are surrounded by a vacuum jacket and reflector to minimize radiative losses. The outer jacket may be water cooled from a constant temperature reservoir to aid temperature stability and to reduce heat flow to the nearby plastic scintillators. The latter system offers better temperature control because the heater current and gas flow may be varied independently. Temperatures up to 800°C have been achieved by Arrott et al. at TRIUMF.

9. The Dependence of Asymmetry on Beam Dynamics and Target Parameters

A muon channel in relation to the pion production target is shown in Figure 2. Along the flight path, which may vary from 2 m to 8 m, pions decay into muons according to expression (7) with 100% polarization in the pion center of mass frame. The degree of polarization in the laboratory frame

13

depends on the angle of the decay cone (determined by the field strength in the channel), the momentum slice selected by the bending magnet, and the subsequent collimation. As less energetic muons are selected, the polarization of the beam is expected to increase since the lower energy muons in the laboratory frame correspond to more directly backward decay of the in-flight pions. Typical cone angles are 35° in the pion center of mass frame and 10° in the laboratory frame.

There are two additional influences on the asymmetry which are determined by the degrader and sample thickness. Because of the beam dynamics just described, decreased degrader thickness tends to increase the muon polarization because only the lower momentum muons are stopped in the sample, even though the total stop rate may be reduced. If the sample itself is comparable in thickness to the range straggling of the beam, decreasing the degrader thickness may increase the asymmetry significantly.

The second effect is due to the energy dependence of the asymmetry in the muon decay spectrum since the high energy positrons have the greater intrinsic asymmetry, Figure 1b. Therefore, increased sample thickness has a beneficial effect in absorbing a larger number of lower energy positrons. When small samples are used, graphite is sometimes used in front of the positron detector to accomplish the same thing. We now give some quantitative measurements of these effects.

A 0.3 cm thick copper target was used to measure the asymmetry by fitting the expression in Equation 7. The resulting asymmetry vs. degrader thickness is plotted in Figure 8. Increased degrader thickness corresponds to stopping initially higher energy muons which have a greater forward component of decay momentum in the lab frame. Thus, one would expect the observed decrease in

14

asymmetry with degrader thickness. The low asymmetry with 2.5 cm of degrader corresponds to stopping very low momentum muons; a significant fraction of which presumably are scattered from the magnets and shielding. With the degrader adjusted for maximum stop rate, these muons are eliminated in normal operation.

It is seen that the effect of reducing the accepted muon decay cone in the channel by allowing lower energy muons, i.e., those emitted more directly backward, to stop in the sample is to significantly increase the asymmetry by increasing the polarization of the beam. The potential benefit of this optimization must, of course, be weighed against a possible reduction in beam rate in each particular installation.

To measure the second effect a 3.8 cm sheet of graphite absorber was placed in front of a 90° positron detector. By comparing the resulting increased asymmetry with the reduction in count rate, due in both cases to preferential absorption of lower energy positrons, the advantage to the measurement of the significant experimental parameters can be determined. A test run obtained $aP(0) = .150(16)$ for no absorber compared to a $aP(0) = .165(13)$ for 3.2 cm of graphite. It is evident that little is gained in this particular setup. However, the effect for each target and detector configuration should be tested, because self absorption in the target may be a major factor as is evident in the following discussion.

It has been noticed through numerous experiments that there seems to be a dependence of asymmetry on the atomic number of the sample material. To test this Z dependence, the asymmetries from six samples (Be, Al, V, Cu, Pb and U) of the same mass thickness were measured. Slight adjustments in degrader were used to maximize the stop rate in the sample, but all other parameters were

15

held fixed. Two different thicknesses of Cu, 5.5 g/cm² and 9.3 g/cm² gave
identical asymmetries with this system verifying that the effect of the small
degrader changes is negligible for these thick samples. The results are shown
in Figure 9. A possible explanation for the observed reduction in asymmetry
with Z lies in the energy dependence of large angle scattering of positrons in
the sample. This derives from the following considerations:

a) The critical energy, E_c, above which bremsstrahlung becomes the
   dominant energy loss mechanism over ionization is inversely
   proportional to Z: $E_c = 1600 \ mc^2/Z.$[21]

b) The magnitude of scattering angle is very strongly dependent on the
   Z of the material in electron scattering from heavy nuclei.[22]

The consequence of this increase in scattering angle with Z for higher
energy positrons is that the higher asymmetry positrons are preferentially
scattered in the sample resulting in the dispersion of their initial decay
direction. Thus, the decay asymmetry is effectively spread out and the
resulting asymmetry in the measured oscillations is reduced with higher Z
samples.

10. Event Rates and Optimization

A. Data Collection Rates

Without going into further details of the experimental arrangement
it is useful to see how one might maximize the data rates of μSR
experiments. In this discussion we need to consider two types of experiments
separately. In the standard setup the stopping muons are individually
observed with rejection events corresponding to either multiple muon stops or
positrons detected within 3 or 4 μ^+ lifetimes on either side of the muon

stop. In the other setup the incoming muons are modulated in time but not individually observed. This latter stroboscopic technique has been used successfully by Schenck and others at SIN.[23]

To establish an upper limit for a practical data rate in the standard arrangement we can define $P(1\mu)$ as the probability that a given μ^+ stopped in the sample does not have another in a time interval $\pm t$. This is the same probability that no additional muons arrive in an interval $2t$ which, if R is the μ^+ stop rate, can be written:

$$P(1\mu) = e^{-R2t} \tag{11}$$

The event rate E is then

$$E = DR (1 - e^{-t/\tau_\mu}) e^{-2Rt} \tag{12}$$

where D is the detection efficiency for the e^+, including solid angles. If we allow $t = 3\tau_\mu$ and $D = 1$ (a number which can be at least approached)

$$E = R(1 - e^{-3}) e^{-6R} \tag{13}$$

If E is maximized with respect to R

$$R = 1/6\tau_\mu = 7.5 \times 10^4 \ \mu^+ \text{ stops/sec,} \tag{14}$$

and

$$E = 2.8 \times 10^4 \text{ events/sec.} \tag{15}$$

It may be interesting to note that if R is dropped to 5×10^4/sec E is reduced to only 2.5×10^4/sec. This lower stopping rate may in practice be a better estimate because of other sources of background. (For example, for some configurations, e^+ traveling in the opposite direction from the incoming μ^+ would also appear as stops.) Further, this 50% decrease in stopping rate has only a 10% effect on the event rate. Thus, a maximum reasonable usable stopping rate is about 5×10^4/sec. producing an event rate of 2.5×10^4/sec. It may be noted that surface beams provide somewhat higher flux and have the advantage of a range of only about 30 mg/cm^2.

17

Stroboscopic methods can utilize the full intensity of the modern machines, but must use fast muons as slower muons lose the required phase coherence within a beam pulse. A 900 mA proton beam will lead to 1.7×10^6 μ^+ stops per gram. Nevertheless, it does give event rates sixty times that of nonstroboscopy. Further, if samples of 30 grams can be obtained, it allows a thousandfold increase in data rate. The upper limit is dictated by electronics considerations, typically it is 10^8 muon stops per second.

Longitudinal field studies are in general subject to the same count rate considerations of the nonstroboscopic method; however, it often happens that the time dependence is sufficiently slow that a structured beam could be used. For example, if the muons arrive in 100 ns pulses separated by 20 µs one could again use much higher average intensities, limited only by the electronics. Of course, the depolarization structure would be convolved with the 100 ns beam burst time.

B. New Fast Timing Techniques

Fortunately, several new methods of charged particle detection look promising for greatly improved timing resolution. The silicon surface barrier solid state detector is presently being made in large enough cross sections and is thin enough to be useful in detecting both the muon and the positron in the same detector. The inherent timing resolution currently available is estimated to be approximately 100 ps, which is compatable with the best presently available constant-fraction discriminators .

Using the conventional photolithographic techniques of present-day technology, multi-element arrays of detectors can be fabricated on a single silicon wafer. With corresponding data storage arrays in the data acquisition

system, an experiment could track the particle trajectories enabling the muon stopping region to be pin-pointed with good accuracy. The conventional limits of beam pile-up rejection would apply to only local regions of the sample, permitting the experiment to make use of the much higher overall stop rates. In some experiments, for example, in the detection of the muonium hyperfine precession frequency, a somewhat higher background causes no serious problems. The higher data rates would in fact be needed in order to offset the lower probability of recording events when the experimental time window is much shorter than the muon lifetime. It is likely that the development of fast semiconductor devices will continue to surpass the fastest photo-multipliers, which with high gain and a small area of cathode illumination have presently achieved a resolution of about 300 ps.

Another device whose promise as a fast charged particle detector still awaits application in μSR is the multi-channel plate detector. This device consists of arrays of channels 15 to 50 μm in diameter, where secondary electron multiplication occurs in the channel walls when a strong longitudinal electric field is applied. High gain and risetimes less than 200 ps have been reported for microchannel plates.

An improvement on the data acquisition system described in Figure 5 makes use of a very high frequency clock to directly digitalize the time interval between the muon stop signal and that from the decay positron. Clocks now available in the 1GHz range would permit 1 nsec resolution and offer the clear advantage of eliminating the analog step in the TAC-ADC system.[24] As higher data rates become possible, the dead time in multichannel analyzers becomes intolerable.

Microprocessor technology has not yet been applied to making the fast integrated logic devices which would be useful in these applications. The pace of innovation is hard to predict, but it is likely that faster discriminator and logic devices with monolithic design would be incorporated into the μSR instrumentation of the future.

11. Conclusion

We have given a brief review of the important experimental factors which must be considered in planning a μSR experiment and shown several measurements that can be made to optimize effective data collection. As in any rapidly developing field, new techniques are constantly being applied; however, the basic simplicity of the experimental design should remain.

References

[1] J. H. Brewer, K. M. Crowe, F. N. Gygax, and A. Schenck, Muon Physics, ed. by V. H. Hughes and C. S. Wu, Academic Press, New York (1975).

[2] A. Schenck, Nuclear and Particle Physics at Intermediate Energies, ed. by J. B. Warren, Plenum, New York (1976).

[3] Muon beams are now available at LAMPF, Los Alamos, New Mexico; TRIUMF, Vancouver, British Columbia; SIN, Villigen, Switzerland; CERN, Geneva, Switzerland; and JINR, Dubna, USSR. The installation of a muon channel at the Brookhaven AGS is planned for early 1982.

[4] H. Fraunfelder and E. Henley, Subatomic Physics, Prentice-Hall (1973).

[5] E. Segré, Nuclei and Particles, W. A. Benjamin, Inc., New York (1964) 601.

[6] V. G. Grebinik, I. I. Gurevich, V. A. Zhuhov, I. G. Ivanter, A. P. Manych, B. A. Nikolskii, V. I. Selivanov and Suetin. JETP Lett. 23, (1976) 8.

[7] I. I. Gurevich, E. A. Meleshko, I. A. Maratova, B. A. Nikolskii, V. S. Roganov, and Selivanov, ZhETF Pis. Red. 18, (1976) 608.

[8] D. G. Fleming, D. M. Garner, L. C. Vaz, J. H. Brewer, and K. M. Crowe, Muonium Chemistry - A review, Advances in Chemistry 175 (1979) 279.

9) J. Fox, R. C. Cohen, A. M. Sachs and E. Zavattini, to be published.

10) A. E. Pifer, T. Bowen and K. R. Kendall, Nucl. Instru. and Meth. 135 (1976) 39.

11) H. W. Reist, D. E. Casperson, A. B. Denison, P. O. Egan, V. W. Hughes, F. G. Mariam, G. Zu Putlitz, P. A. Souder, P. A. Thompson and J. Vetter, Nucl. Instr. and Meth. 153 (1978) 61.

12) M. Camani, F. N. Gygax, E. Klempt, W. Ruegg, A. Schenck, H. Schilling, R. Schulze, H. Wolf, Hyperfine Interactions 6 (1979) 33.

13) K. W. Kehr, D. Richter, G. Honig, Hyperfine Interactions 6 (1979) 219.

14) K. Petzinger, R. Munjal, E. Zaremba, to be published.

15) W. J. Kossler, A. T. Fiory, W. F. Lankford, K. G. Lynn, R. P. Minnich and C. E. Stronach, Hyperfine Interactions 6 (1979) 295.

16) T. Yamazaki, Hyperfine Interactions 6 (1979) 115.

17) R. S. Hayano, Y. J. Uemura, J. Imazato, N. Nishida, T. Yamazaki, and R. Kubo, Phys. Rev. B 20 (1979) 850.

18) J. A. Brown, R. H. Heffner, M. Leon, S. A. Dodds, D. A. Vanderwater, and T. L. Estle, Phys. Rev. Lett., 43 (1979) 1751.

19) R. H. Haffner, Private Communication.

20) O. Hartman, E. Karlsson, L. O. Norlin, T. O. Niinikoski, K. W. Kehr, D. Richter, J. M. Welter, A. Yaouanc, and J. LeHericy, Phys. Rev. Lett. 44, (1980) 337.

21) H. A. Bethe and W. Heitler, Prac. Roy. Soc. A146 (1934) 83.

22) C. S. Wu and C. L. Yuan, Methods of Experimental Physics Vol. 5 Academic Press (1961) 68.

23) M. Camani, F. N. Gygax, E. Klempt, W. Ruegg, A. Schenck, H. Shilling, R. Schulze, and H. Wolf, Phys. Lett. 77B, (1978) 326.

24) G. Lenzi, P. Rodini, R. Reverberi, and K. Pernestal, Nuc. Instr. and Meth. 150, (1978) 575.

Table I

Comparison of μ^+ fluxes at intermediate energy proton machines.

Facility	CERN Switz.	TRIUMF B. C.	SIN Switz.	LAMPF N. M.	BNL N. Y.
Proton current (µA)	4	20	80	300	2×10^{12} protons per pulse
μ^+ Momentum (MeV/c)	124	50	120	130	200
μ^+ Flux (sec^{-1} cm^{-2} µA^{-1})	50	60	2×10^5	8	7×10^7 total muons per 10^{12} protons

Table II

Comparison of 30 MeV/c surface muon fluxes.

Facility	SIN	TRIUMF	LAMPF
Proton current (µA)	1000	20	300
μ^+ Flux (sec^{-1}cm^{-2} µA^{-1})	4×10^5(a)	200	4000

(a) Calculated for proposed beam

FIGURE CAPTIONS

Fig. 1   a) Positron decay asymmetry.

b) Energy dependence of decay positrons.

Fig. 2   Layout of a muon channel in relation to the pion production target.

Fig. 3   Production geometry for a surface muon beam.

Fig. 4   A typical detector arrangement for µSR experiments where the applied

magnetic field is transverse to the beam direction. A B2 M F signal

specifies a stopped muon and a subsequent A or an F specifies the

decay positron. An additional detector at 90° to the beam (not

shown) may also be used.

Fig. 5   Logic diagram for transverse field µSR experiments.

Fig. 6   A µSR time spectrum illustrating the precession oscillations and

depolarization for three different temperatures. The sample was

vanadium. The exponential decay of the muon has been removed and the

background subtracted from the data.

Fig. 7   A typical longitudinal field arrangement for µSR experiments.

Fig. 8   Asymmetry in the oscillations of the positron time spectrum vs.

degrader thickness. The target was 1/8" thick Cu disk. Positron

detectors at $\theta = 0^\circ$, 90° (with respect to forward beam direction).

Fig. 9   Initial asymmetry vs. atomic number of target material, 90° and 0°

positron detector averages.
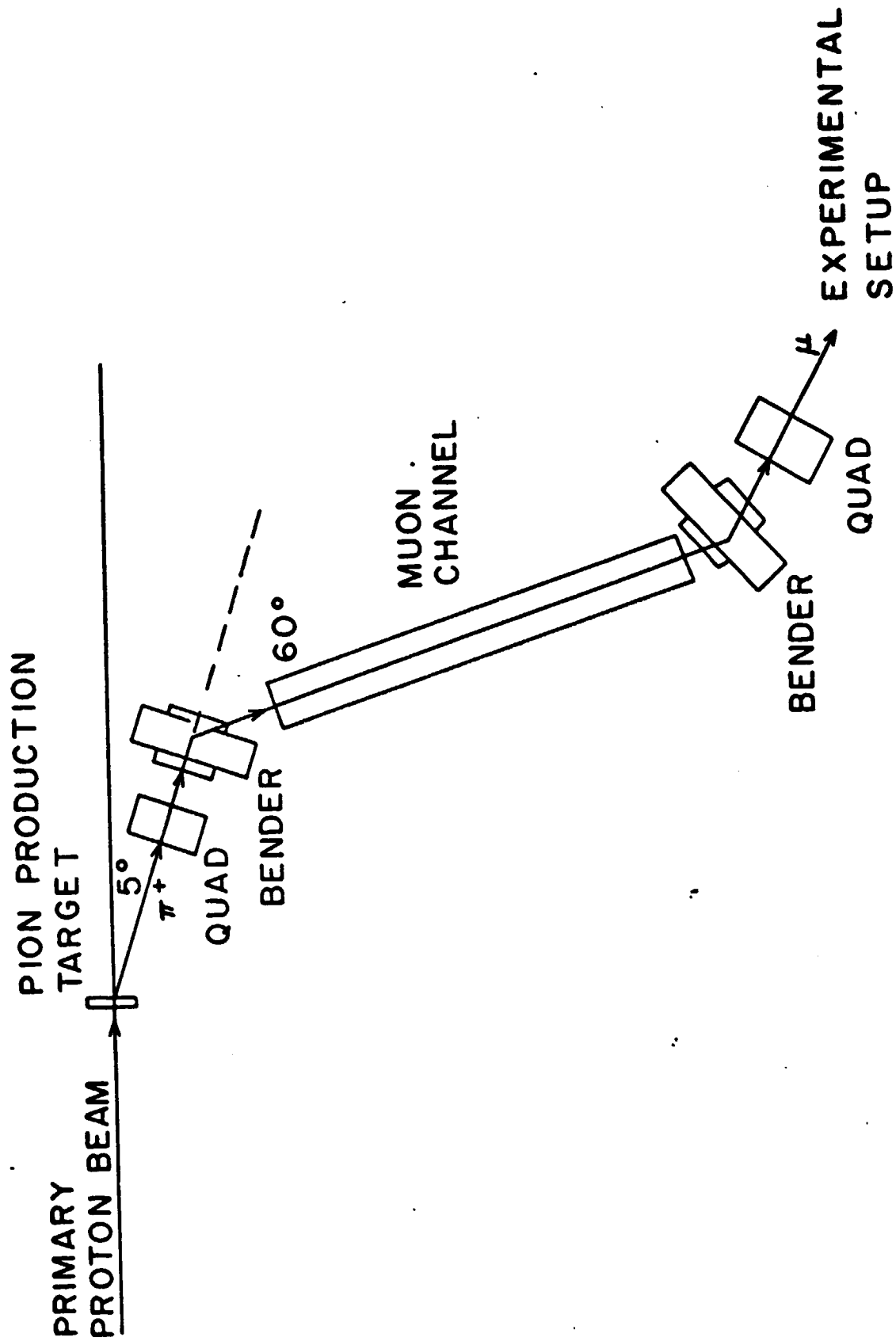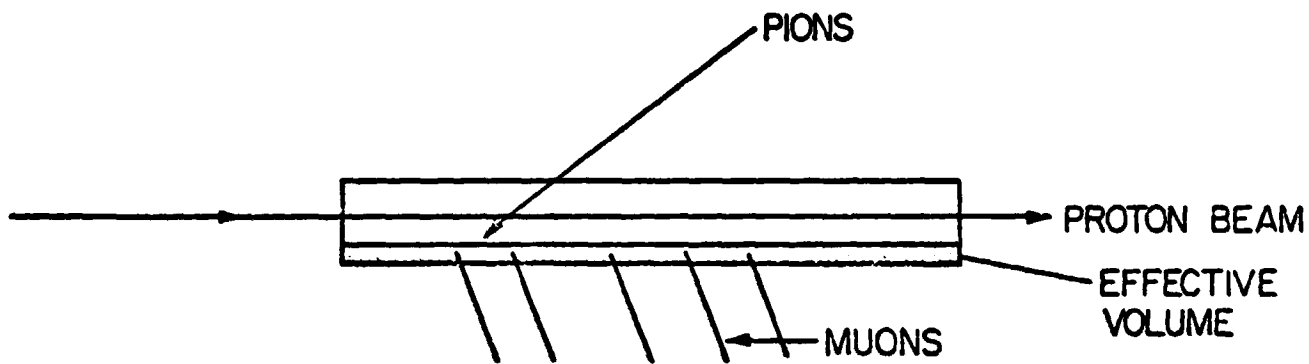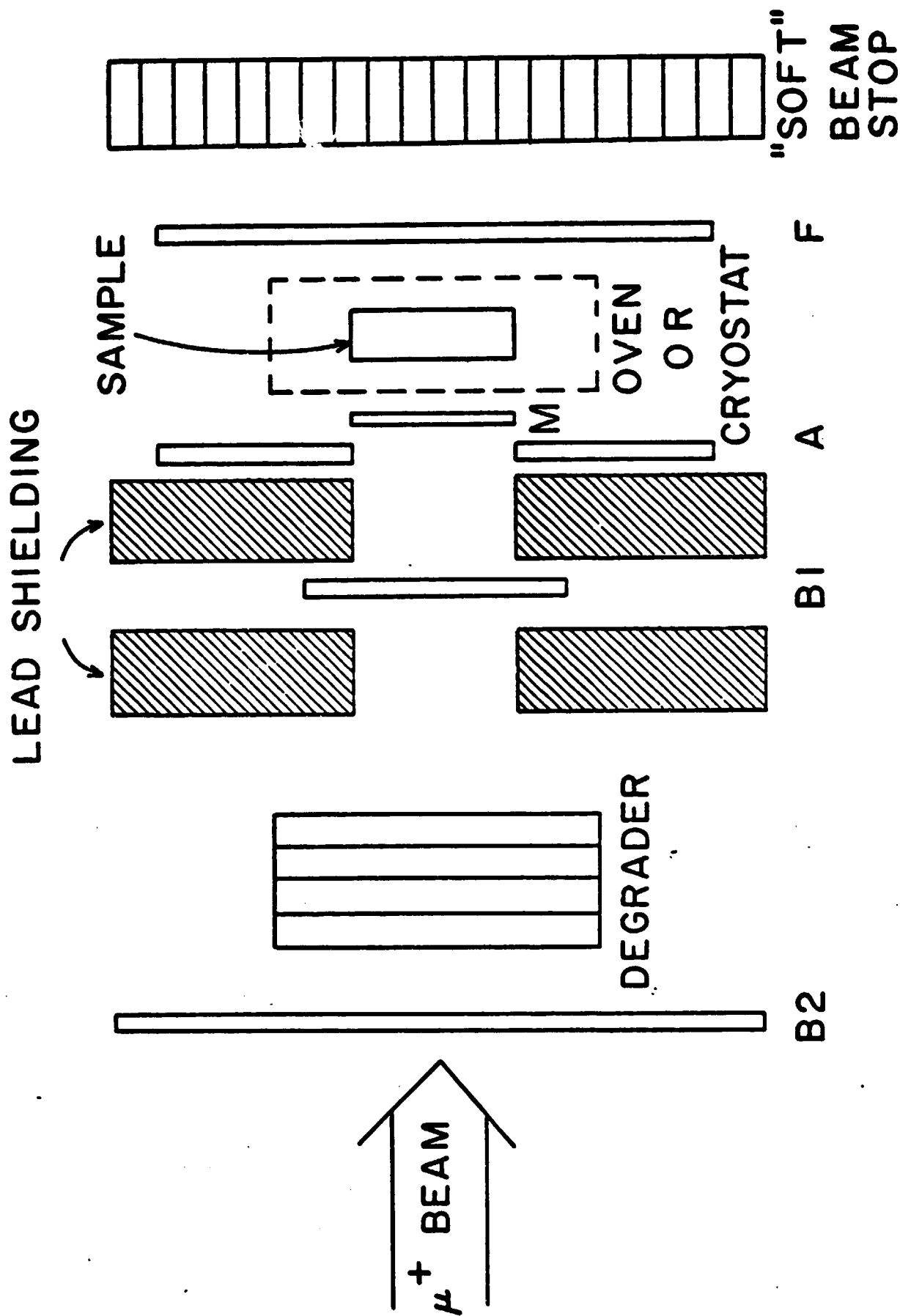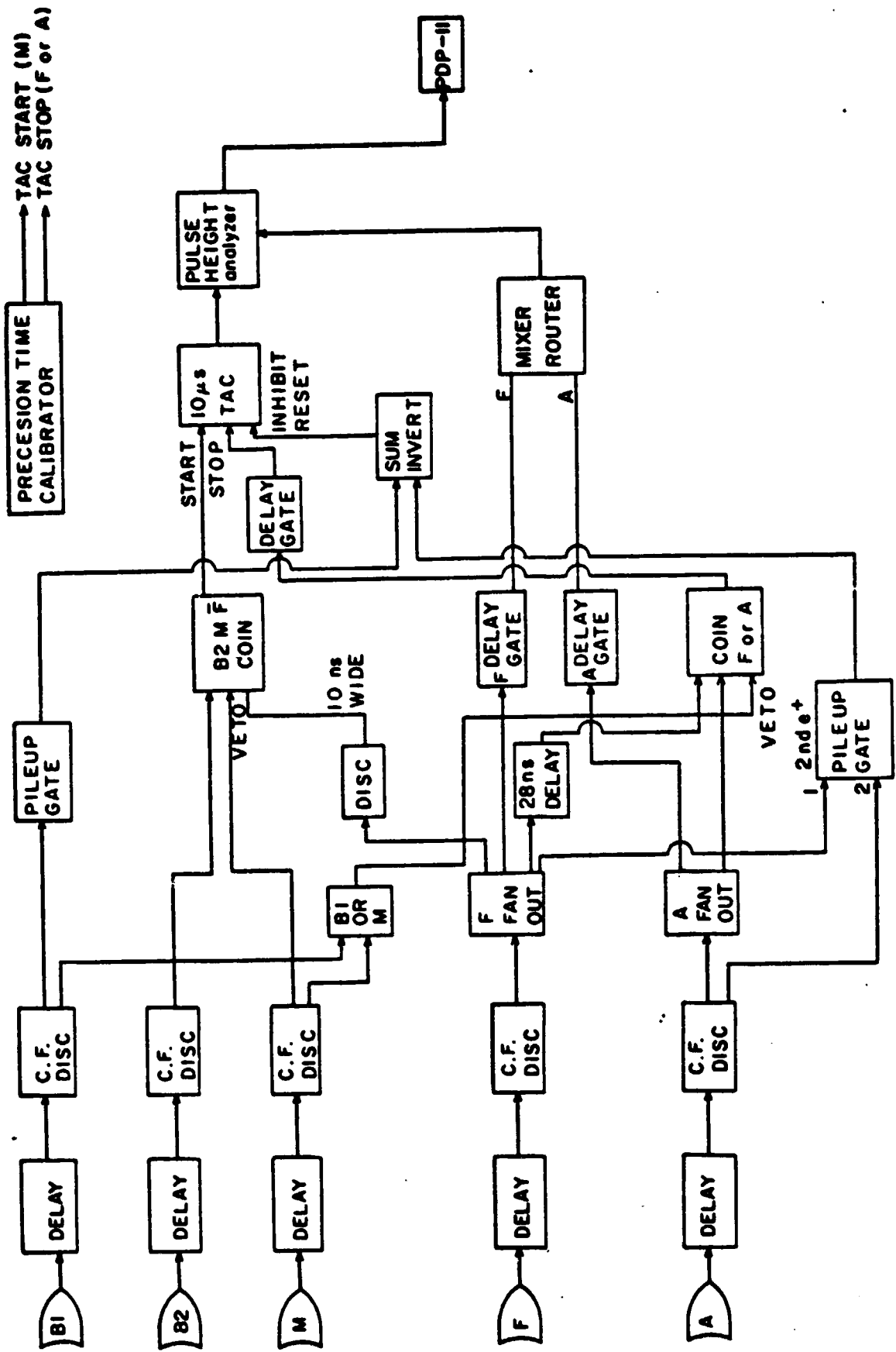
$R(\theta) = 1 + 1/3 \cos \theta$

Fig. 1 b.

PRIMARY PROTON BEAM

PION PRODUCTION TARGET

5°

π^+

QUAD

BENDER

60°

MUON CHANNEL

BENDER

QUAD

μ

EXPERIMENTAL SETUP

Fig 2

PIONS

PROTON BEAM

EFFECTIVE VOLUME

MUONS

LEAD SHIELDING

SAMPLE

OVEN OR CRYOSTAT

"SOFT" BEAM STOP

DEGRADER

μ^+ BEAM

F A B1 B2

M

F̴. ıL

COIL

COIL

COIL

COIL

F M

A A

LEAD
SHIELDING

B1

B2

μ^+ BEAM

z

y

x

ANNULAR (3cm CENTER BLANK)
POSITRON DETECTORS
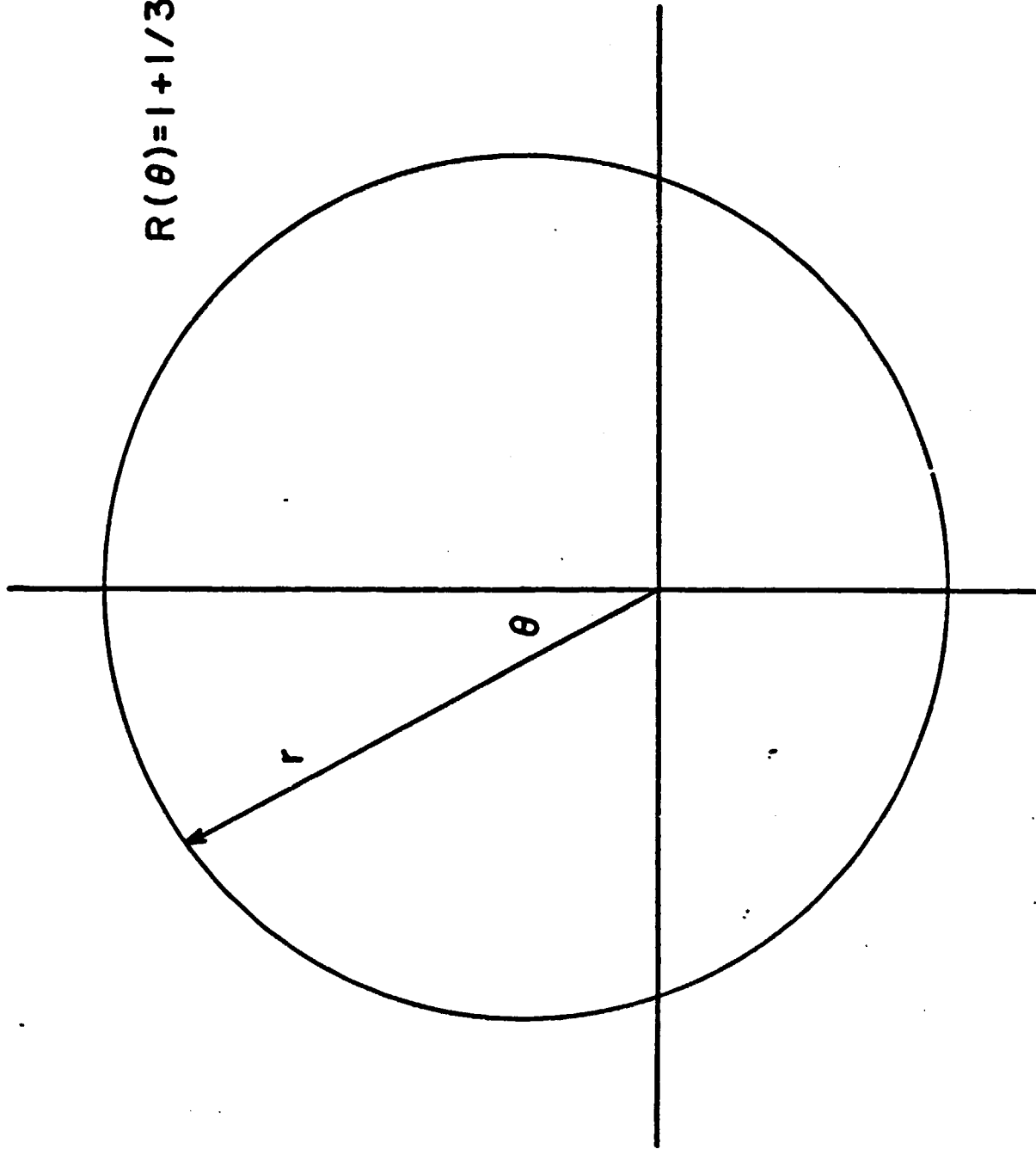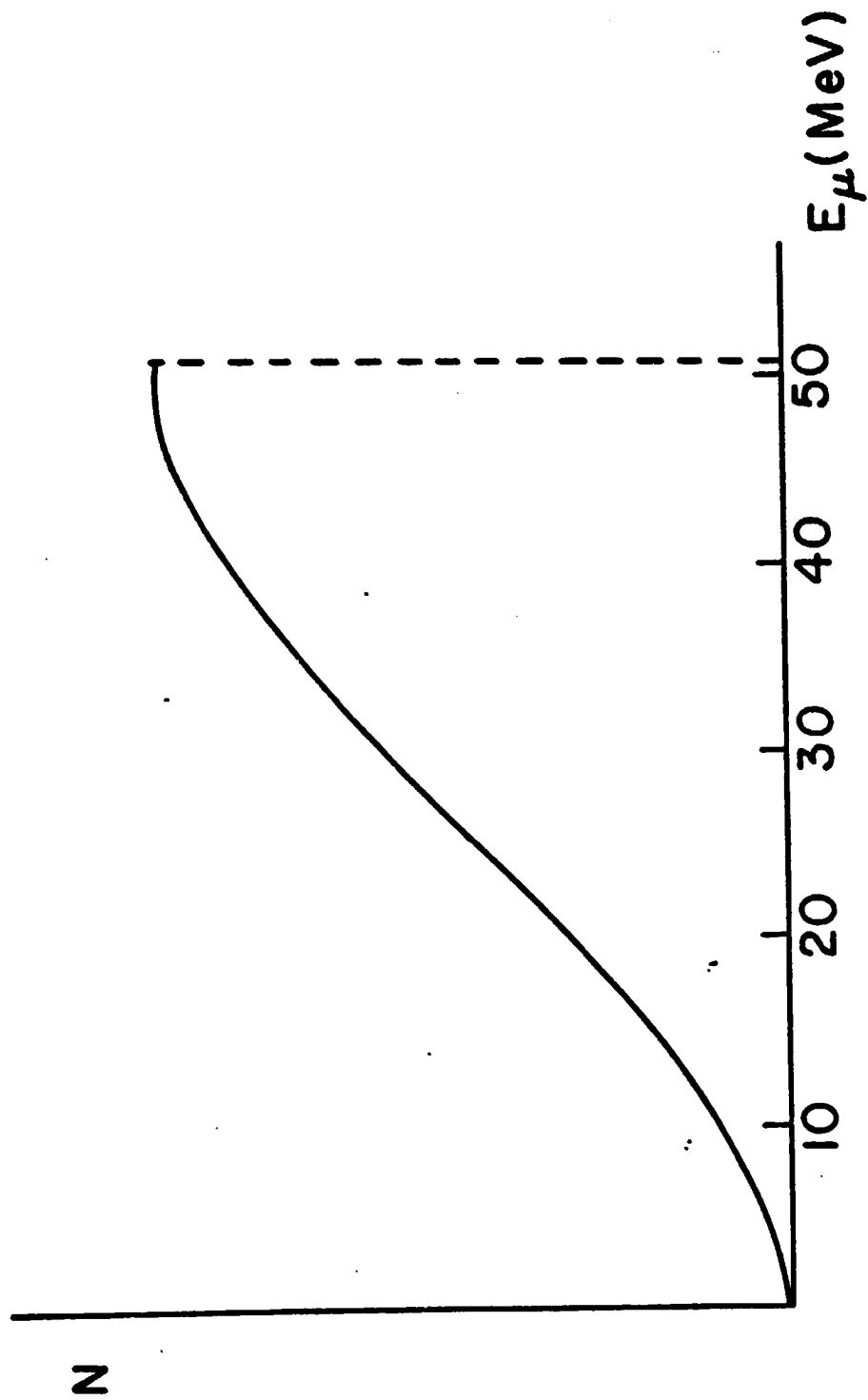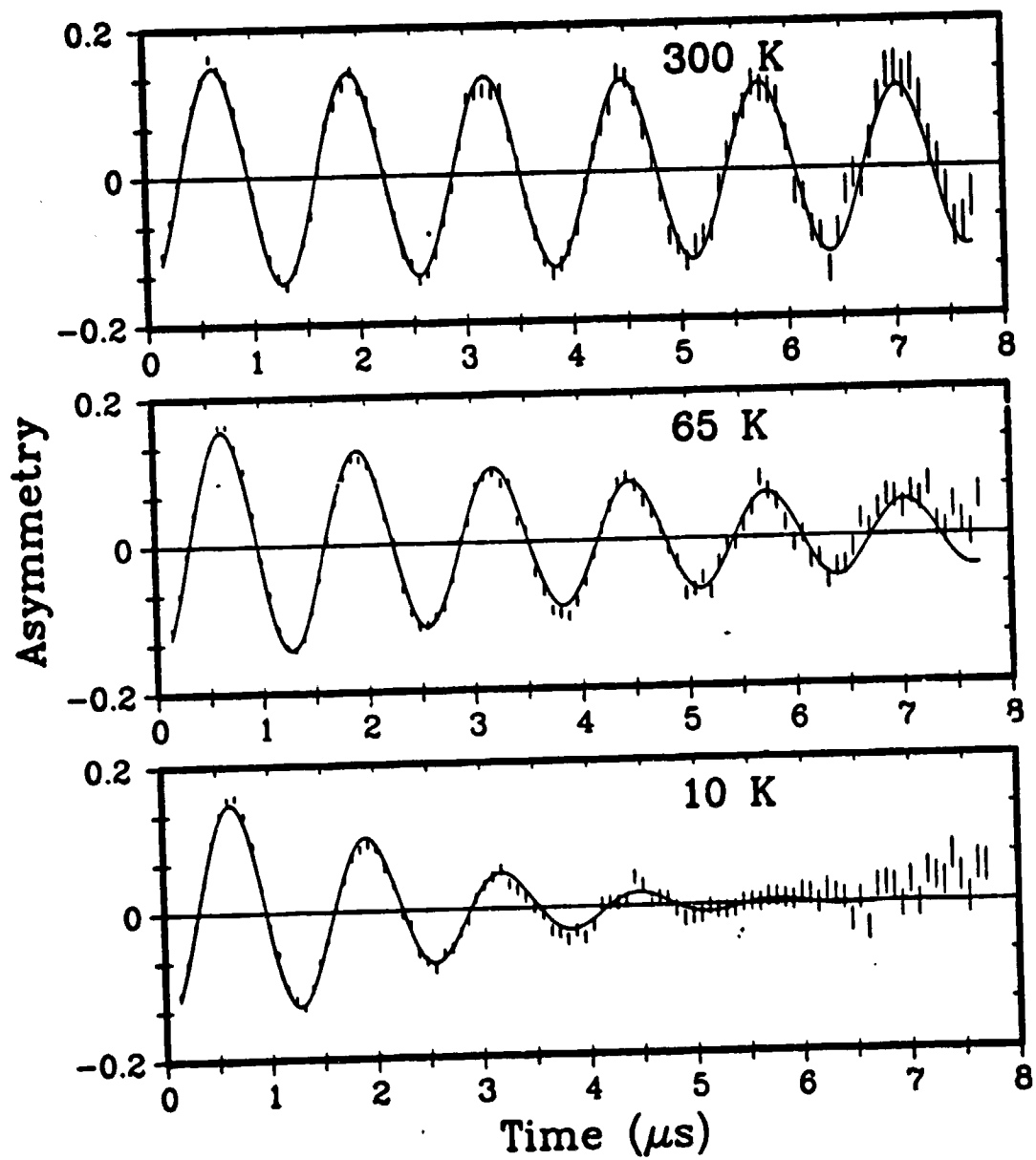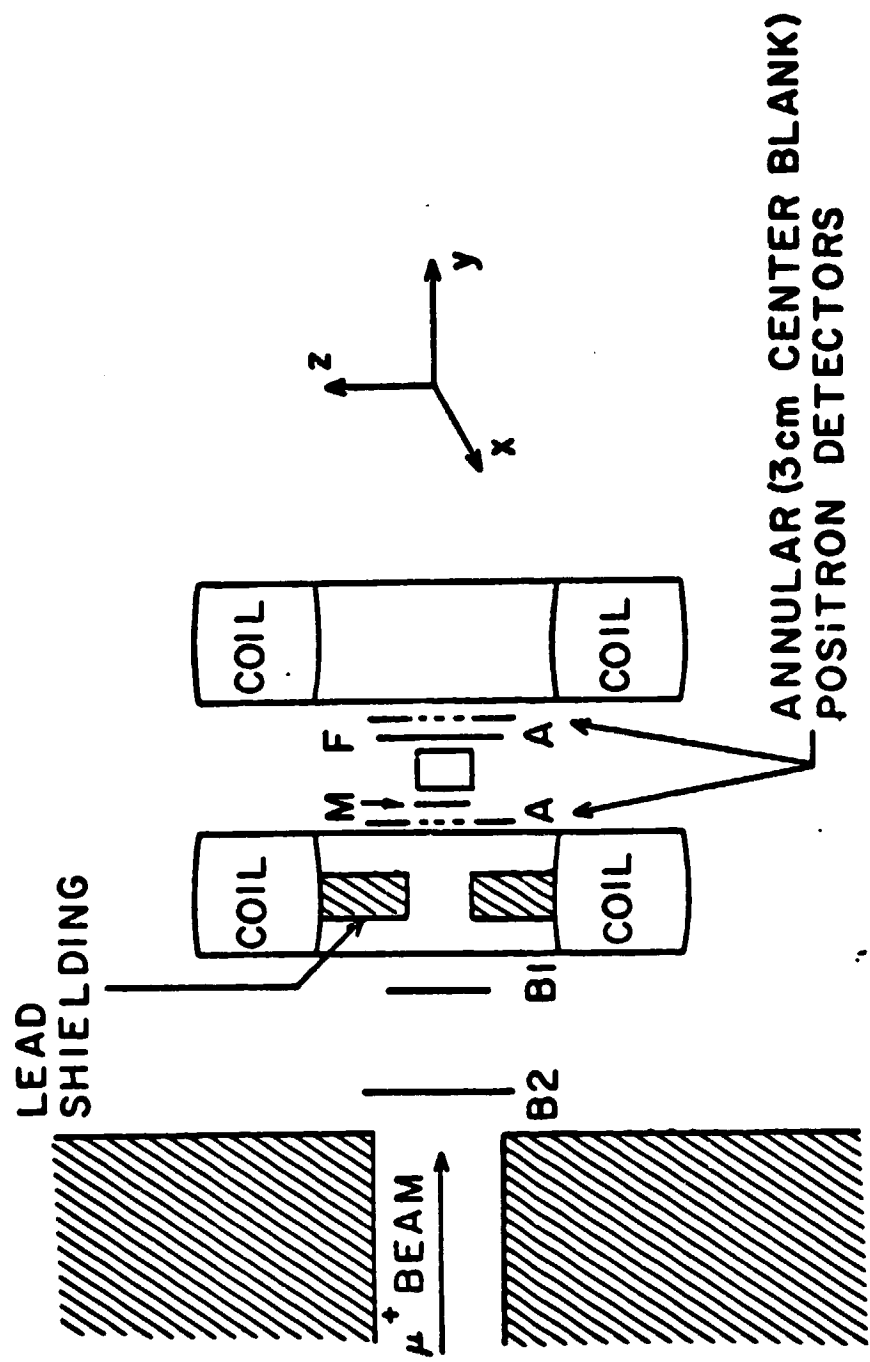
APPROX. SCALE

0   4cm

Fig 8

Fig 9